FIBER-MATRIX DEBONDING BEHAVIOR USING IN-SITU ELECTRON AND LIGHT MICROSCOPY DURING MECHANICAL TESTING

Olivier Verschatse[1], Mehdi Nikforooz[2], Karen De Clerck[1], Wim Van Paepegem[2] and Lode Daelemans[1]

[1]Ghent University, Department of Materials, Textiles and Chemical Engineering (MaTCh), Centre for Textile Science and Engineering (CTSE), Technologiepark 70 9052 Zwijnaarde, Belgium
Email: Lode.Daelemans@UGent.be, Olivier.Verschatse@UGent.be, Karen.DeClerck@UGent.be
Web Page: https://textiles.ugent.be
[2] Ghent University, Department of Materials, Textiles and Chemical Engineering (MaTCh), Mechanics of Materials and Structures (MMS), Technologiepark 46 9052 Zwijnaarde, Belgium
Email: Wim.VanPaepegem@UGent.be, Mehdi.Nikforooz@UGent.be
Web Page : https://composites.ugent.be

Keywords: DIC, SEM, interface, microstructural, microscale

Abstract
This study visualizes the interface debonding phenomenon in glass/epoxy composite materials through an approach combining in-situ scanning electron microscopy (SEM) and (polarized) light microscopy (POM) techniques during mechanical testing of small-scale specimens. This allows for real-time observation and detailed analysis of the debonding process at the microscale. We also introduce a simple microscale speckling technique to analyze strain distribution on SEM images during debonding using digital image correlation. By employing thin cruciform-shaped single fiber composite specimens, the full interface length could be analyzed with light microscopy, revealing insights into debond initiation and propagation under normal loading conditions. This approach allows to quantify the remote stress level initiating debonding. Our findings offer a deeper understanding of microscale debonding behavior and could be used to determine quantified data for micromechanical finite element models. This research presents a comprehensive framework adaptable for studying diverse composite materials, providing both potential and limitations for microscale analysis.

1. Introduction

The interface between fibers and matrix is a key component that determines the performance of fiber reinforced composites as the interface quality significantly influences the composite's behavior and properties. To evaluate the interface strength, various methods can be used, including the microdroplet test, fragmentation test, and fiber pull-out test [1–7]. These tests primarily assess adhesion strength under shear loading, whereas composites often fail under normal or mixed-mode stress at the fiber-matrix interface.

To address this limitation, several tests have been proposed, such as the Broutmann test [8], the transverse tensile test [9–12] and the cruciform single fiber test [13–16]. The latter method is very similar to the single fiber fragmentation tests, except that the fiber is now positioned at 90° (instead of 0°) to the tensile direction. The cruciform shape is necessary to introduce a central zone of homogeneous stress and circumvent any stress concentrations near edges which would occur in rectangular specimens. By observing debonding initiation and propagation, values for interface strength could be determined.

In this study, we produced thin, void-free samples containing a single fiber through a small-scale vacuum assisted resin transfer moulding setup. In addition, an improved cruciform sample design was

used which had a thinned gauge area to maximize the stress acting on the embedded fiber. The thin samples enable clear observation of the debonding process using both normal and polarized light microscopy.

2. Materials and methods

The epoxy resin used was Epikote™ Resin MGS RIMR 135, based on diglycidyl ether of bisphenol A (DGEBA), and it was combined with a liquid diamine hardener, Epicure™ Curing Agent MGS RIMH 137, from Momentive Specialty Chemicals. Both components were mixed in a 100:30 weight ratio and degassed in a vacuum desiccator for 10 minutes. After curing, 24 hours at room temperature followed by 15 hours at 80°C, the epoxy system achieves a glass transition temperature between 80 and 90°C. This curing process is commonly used in the production of wind turbine blades, making it relevant for study. Two types of E-glass fibers from Johns Manville were used. One type had epoxy-compatible sizing (StarRov® PR 220 1200 090), and the other had epoxy-incompatible sizing (StarRov® PR 220 1200 490). Both fibers have a nominal filament diameter of 16 µm.

Specimens containing a single fiber were made through a small-scale vacuum assisted resin transfer moulding setup. The mould was constructed from glass plates and resin was infused through very small tubing. Stackable spacers were used to guarantee a controllable thickness ranging from 200 to 1500 µm.

Via the use of an in-house designed tensile stage integrated into an optical microscope, it was possible to study the fiber-matrix interface both in reflection and transmission mode (**Figure 1**). By using a step-and-shoot method (5 N steps, 0.75 mm/min for a 15 mm gauge length), the complete fiber-matrix interface across the entire gauge area could be scanned and recorded allowing for subsequent analysis. Due to the translucency of the thin (approx. 200 µm) specimens, any fiber-matrix debonding is visible on the microscopic pictures as black lines or spots which represent the location of the fiber where debonding occurs, see **Figure 2**.

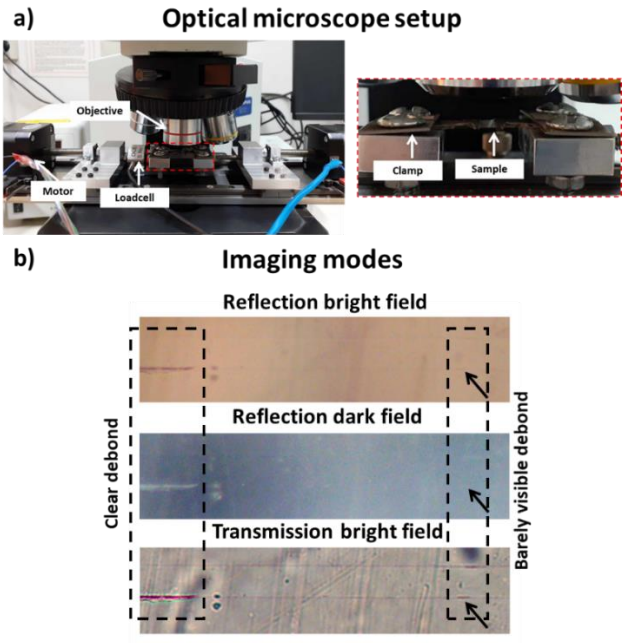

Figure 1. (a) Overview of the test setup. An Olympus BX-51 microscope was used with an in-house made dedicated tensile stage. (b) Via transmission lighting (normal and polarized) the sample could be studied.

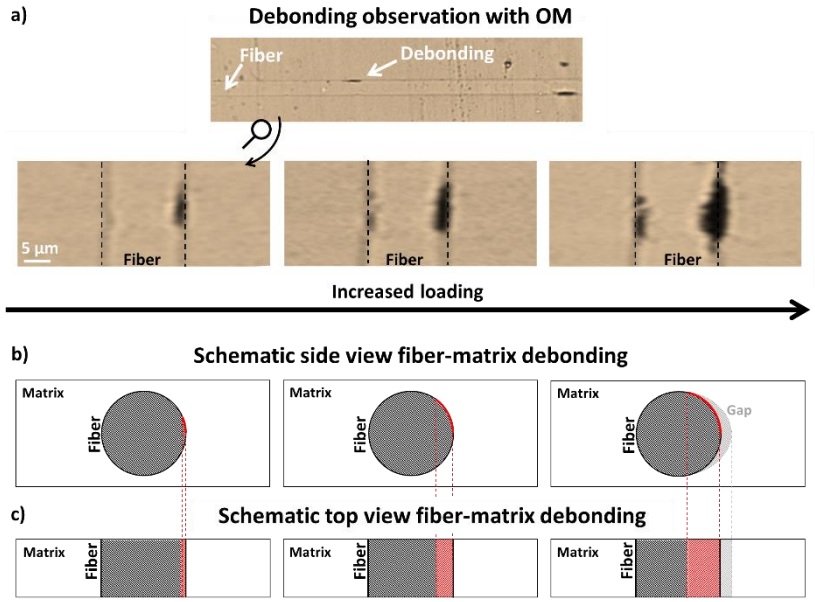

Figure 2. (a) Fiber-matrix debonding is observed as a thin black line at the interface using optical light transmission microscopy. (b and c) Schematical representation of the debond view.

The application of speckles for digital image correlation (DIC) analysis as published in earlier work [17] proved feasible for composite specimens as well. This process involved immersing the samples to deposit a dense layer of carbon-based polymer speckles. As the particles don't (visually) shield the surface from the electron beam, they allow to clearly observe matrix deformation and fiber-matrix debonding.

Single fiber composite beam samples were prepared using the small-scale vacuum-assisted resin transfer molding. Samples, ranging from 4 to 6 mm in width and approximately 1.50 mm in thickness, were cut, ground and polished before undergoing the speckle application and in-situ SEM testing. A gold coating was applied to enhance conductivity before positioning them in a tree point bending (3PB) testing setup with a 15 mm span length (**Figure 3**). The fibers were oriented at 90° in the beam sample, perpendicular to the surface visualized by SEM (Phenom XL, 5 kV accelerating voltage).

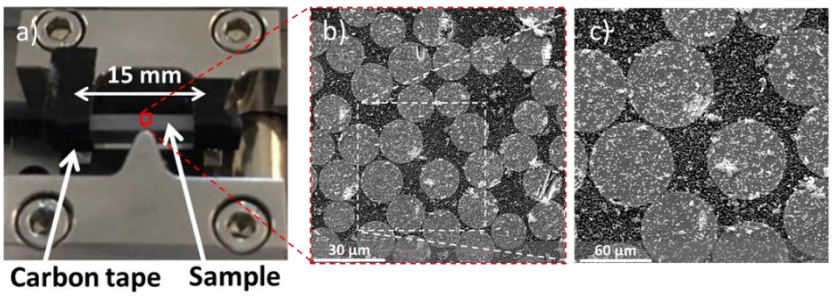

Figure 3. (a) Three-point bending setup integrated in SEM specimen holder. (b and c) SEM image of a composite specimen with the microscale speckle pattern applied for DIC measurements.

3. Results and discussion

3.1 Fiber-matrix debonding visualized by in-situ polarized optical microscopy

Two fibers were analyzed for their fiber-matrix debonding, one with a compatible sizing for epoxy and one with an incompatible sizing as provided by the manufacturer. For each fiber type, multiple single fiber cruciform specimens were produced and the debonding behavior analyzed from microscopic pictures. This was done by incrementally increasing the load on the specimen and creating a stitched microscopic image over the full length of the embedded fiber. The amount of debonds and also their length were subsequently measured using ImageJ.

The fiber-matrix debonding progression was clearly different between the compatible and incompatible sizing, especially in terms of debond propagation. Indeed, debond initiation was seen to occur for both fiber types already at quite low remote stress levels (approx. 10 MPa). For increased loads, the debond sites in the fibers with compatible sizing barely increased in length indicating limited debond propagation, while more initiation sites start to occur over the full length of the fiber (**Figure 4**). Only at very high remote stress levels, the debonds are seen to propagate along the full length of the fiber.

For the incompatible sized fiber specimens, the initial behavior was similar, with debonding initiation at relatively low stress levels, but this was quickly followed by rapid propagation of the debonds over the full length of the fiber. The propagation of the debonds was mainly in the longitudinal direction (fiber direction), and almost no radial growth was observed. The radial propagation only occurred at higher remote stress levels (approx. 32 MPa) when already a major part of the fiber has debonded from the matrix.

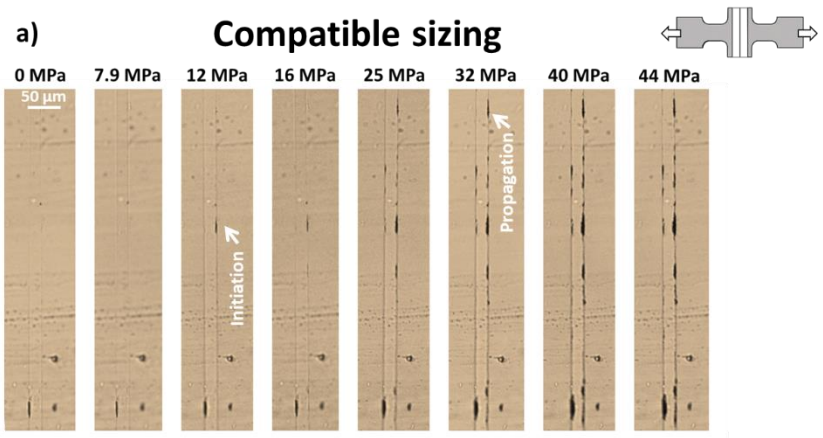

Figure 4. Fiber-matrix debond initiation and limited propagation at different loading levels.

Figure 5 represents the relative debond length (with 100% meaning that the full gauge area has debonded) as measured on the microscope images. It is clear that both incompatible and compatible sized fibers show debond initiation around the same remote stress level (taking in mind that there are already initially some debond sites present due to the fabrication and unmoulding of the specimen). This suggest that initiation might be partially independent from fiber sizing. This could correspond to the presence of a radial compressive stress state induced by the thermal expansion mismatch between the epoxy resin and the fiber material during curing. Nevertheless, after initiation, the difference between the compatible and incompatible sizing is immediately clear by the difference in debond propagation rate.

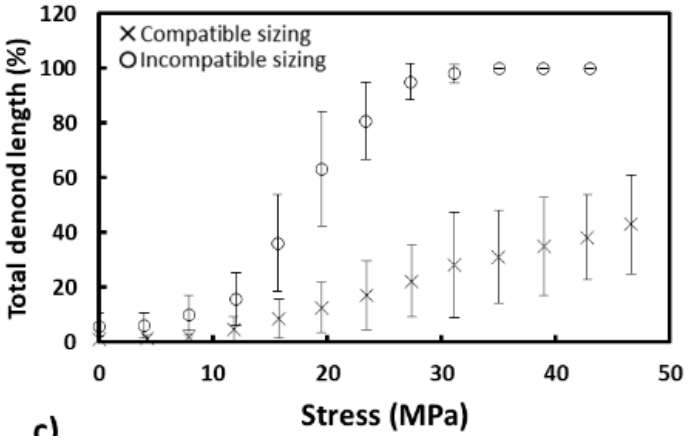

Figure 5. (a) The total debond length (%) for the compatible and incompatible sized fiber specimens.

3.2 Fiber-matrix debonding by in-situ scanning electron microscopy

To visualize the fiber-matrix debonding by SEM, one is limited to surface visualization only. Therefor, straight rectangular beams were produced with a thickness of approx. 1.5 mm in which the fiber was positioned in the center near the surface of the beam. This beam is subsequently loaded in three point bending, with the fiber located above the central roller (**Figure 6**), resulting in a tensile deformation near the fiber. At each load or strain increment level, the region is scanned and the SEM image recorded (as well as the displacement and force data from the tensile tester). The upside of in-situ SEM is the high magnification and quality of the images that allow to very precisely capture the moment of fiber-matrix debonding. The downside however is that the image (and the recorded phenoma) only represents the material locally and on the surface.

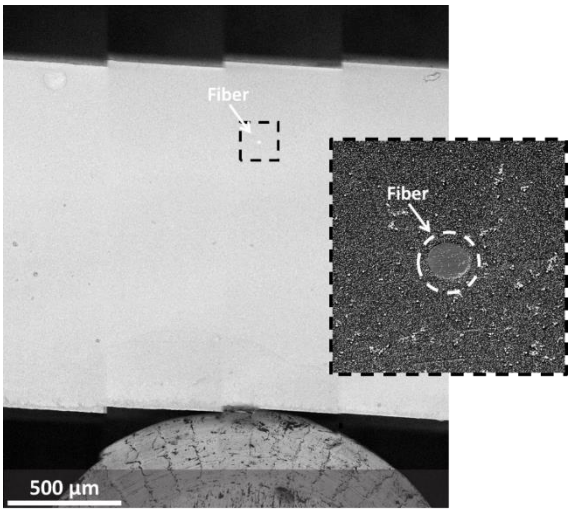

Figure 6. Overview stitched image of a single-fiber composite specimen. The jagged specimen edges are an artefact of the stitching algorithm due to the low image contract. Nevertheless, the stitched image was only used to determine the overall position of the fiber with regards to the surface and loading roller. Subsequent imaging was done without stitching. The insert shows the DIC speckle pattern applied to the specimen.

Upon loading of the specimen, there is a clear strain concentration surrounding the fiber, as should be expected. In addition, the remote strain level by DIC is in accordance with the expected bending strain calculated using the elastic modulus of the material up to approx. 4% of strain (after which plasticity occurs). Similarly to what was observed with in-situ POM, the debond initiation occurs at the fiber edge

at low remote stress levels, after which is grows radially inward. Upon increased loading, there forms a clear gap between the fiber and matrix material which indicates high amounts of plasticity (**Figure 7**).

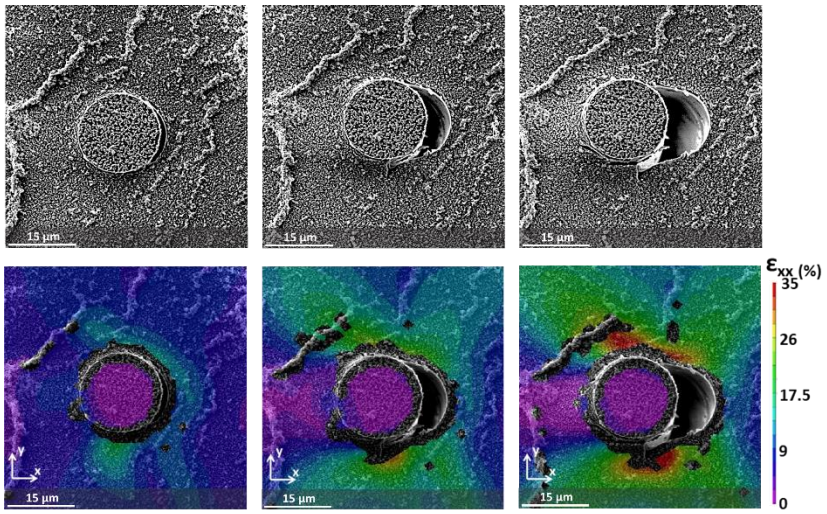

Figure 7. Elongation of the debond gap without kinking of the debond into the matrix. DIC analysis shows the large strain around the debond gap.

4. Conclusions

The combination in-situ SEM and POM aid in the understanding of the fiber-matrix mechanism under normal loading conditions. Our results revealed that for a good fiber-matrix adhesion, initiation of numerous small debonds across the fiber-matrix interface zone occurs. This already occurred at quite low remote stress levels. Upon increased loading, more initiation sites occur, while the existing debonds propagated (especially for the incompatible sizing) and coalesced under increased stress, forming larger debonds.

References

[1] D.A. Jesson, J.F. Watts, The Interface and Interphase in Polymer Matrix Composites: Effect on Mechanical Properties and Methods for Identification, Http://Dx.Doi.Org/10.1080/15583724.2012.710288 52 (2012) 321–354. https://doi.org/10.1080/15583724.2012.710288.

[2] J. Koyanagi, S. Ogihara, H. Nakatani, T. Okabe, S. Yoneyama, Mechanical properties of fiber/matrix interface in polymer matrix composites, Https://Doi.Org/10.1080/09243046.2014.915125 23 (2014) 551–570. https://doi.org/10.1080/09243046.2014.915125.

[3] S. Huang, Q. Fu, L. Yan, B. Kasal, Characterization of interfacial properties between fibre and polymer matrix in composite materials – A critical review, Journal of Materials Research and Technology 13 (2021) 1441–1484. https://doi.org/10.1016/J.JMRT.2021.05.076.

[4] Z. Liu, X. Yuan, A.J. Beck, F.R. Jones, Analysis of a modified microbond test for the measurement of interfacial shear strength of an aqueous-based adhesive and a polyamide fibre, Compos Sci Technol 71 (2011) 1529–1534. https://doi.org/10.1016/J.COMPSCITECH.2011.06.001.

[5] L. Yu, K. Wang, Y. Guan, Z. Liu, M. Sun, Y. Zhao, Effect of carbon fiber surface properties on carbon fiber/polyphenylene sulfide composite interfacial property, Polym Compos 44 (2023) 2005–2015. https://doi.org/10.1002/PC.27224.

[6] L. Yang, J.L. Thomason, Interface strength in glass fibre–polypropylene measured using the fibre pull-out and microbond methods, Compos Part A Appl Sci Manuf 41 (2010) 1077–1083. https://doi.org/10.1016/J.COMPOSITESA.2009.10.005.

[7] J.C. Zarges, H.P. Heim, Influence of cyclic loads on the fiber-matrix-interaction of cellulose and glass fibers in polypropylene, Compos Part A Appl Sci Manuf 149 (2021) 106491. https://doi.org/10.1016/J.COMPOSITESA.2021.106491.

[8] R. Sinclair, R.J. Young, R.D.S. Martin, Determination of the axial and radial fibre stress distributions for the Broutman test, Compos Sci Technol 64 (2004) 181–189. https://doi.org/10.1016/S0266-3538(03)00257-4.

[9] K. Martyniuk, B.F. Sørensen, P. Modregger, E.M. Lauridsen, 3D in situ observations of glass fibre/matrix interfacial debonding, Compos Part A Appl Sci Manuf 55 (2013) 63–73. https://doi.org/10.1016/J.COMPOSITESA.2013.07.012.

[10] R. Livingston, B. Koohbor, Characterizing fiber-matrix debond and fiber interaction mechanisms by full-field measurements, Composites Part C: Open Access 7 (2022) 100229. https://doi.org/10.1016/J.JCOMC.2022.100229.

[11] M. Fichera, K. Totten, L.A. Carlsson, Seawater effects on transverse tensile strength of carbon/vinylester as determined from single-fiber and macroscopic specimens, J Mater Sci 50 (2015) 7248–7261. https://doi.org/10.1007/S10853-015-9279-3/TABLES/9.

[12] K.R. Totten, B. Kutub, L.A. Carlsson, In situ determination of the fiber–matrix interface tensile strength, Http://Dx.Doi.Org/10.1177/0021998315579926 50 (2015) 589–599. https://doi.org/10.1177/0021998315579926.

[13] J. Koyanagi, S. Ogihara, Temperature dependence of glass fiber/epoxy interface normal strength examined by a cruciform specimen method, Compos B Eng 42 (2011) 1492–1496. https://doi.org/10.1016/J.COMPOSITESB.2011.04.041.

[14] J.M. Chu, B. Claus, B.H. Lim, D. O'Brien, T. Sun, K. Fezzaa, W. Chen, Rate effects on fiber–matrix interfacial transverse debonding behavior, J Compos Mater 54 (2020) 501–517. https://doi.org/10.1177/0021998319866904/ASSET/IMAGES/LARGE/10.1177_0021998319866904-FIG18.JPEG.

[15] J. Koyanagi, H. Nakatani, S. Ogihara, Comparison of glass–epoxy interface strengths examined by cruciform specimen and single-fiber pull-out tests under combined stress state, Compos Part A Appl Sci Manuf 43 (2012) 1819–1827. https://doi.org/10.1016/J.COMPOSITESA.2012.06.018.

[16] V.T. Bechel, G.P. Tandon, Modified Cruciform Test for Application to Graphite/Epoxy Composites, Http://Dx.Doi.Org/10.1080/153764902317224842 9 (2010) 1–17. https://doi.org/10.1080/153764902317224842.

[17] O. Verschatse, W. Van Paepegem, K. De Clerck, L. Daelemans, Development of a versatile speckle pattern of nano-sized polymer particles for high-resolution SEM-DIC, Polym Test 125 (2023) 108134. https://doi.org/10.1016/J.POLYMERTESTING.2023.108134.